International Journal of Physics and Applications
Online ISSN: 2664-7583; Print ISSN: 2664-7575
Received: 07-04-2019; Accepted: 08-05-2019; Published: 15-05-2019
www.physicsjournal.in
Volume 1; Issue 1; 2019; Page No. 43-49

The structural, mechanical, electronic, optical and thermodynamic properties of in-based carbide M_3InC (where M=Y and La)

Atikur Rahman Md[1*], MU Salma[2]
[1-2] Department of Physics, Pabna University of Science and Technology, Pabna, Bangladesh

DOI: https://doi.org/10.33545/26647575.2019.v1.i1a.18

Abstract
In this research work, we have studied the structural, mechanical, electronic, optical and thermodynamic properties of antiperovskite compounds M_3InC (where M=Y and La) by using the first-principles calculations method depend on density functional theory (DFT). The optimized lattice parameters are in good accord with the experimental data. The observed elastic constants are positive and prove the mechanical stability for all these phases. Cauchy pressure, Pugh's ratio and Poisson's ratio show the brittleness characteristics for these compounds. The expectation of dislocation movement for both these phases is confirmed from the Peierls stress. The Zener anisotropy factor indicates the anisotropic behavior of M_3InC (where M=Y and La). Bulk modulus and hardness values indicate the softness behavior of Y_3InC and La_3InC. The analysis of the band structure diagrams as well as density of states (total density of states and partial density of states) evidence the metallic behavior for all the compounds. The large reflectivity in the high energy region (8-9 eV) of Y_3InC and La_3InC indicates that these are good promising coating material in the UV energy region. The absorption and conductivity spectra indicate good absorbtivity and conductance in the visible and UV regions. We have also investigated the Debye temperature, minimum thermal conductivity and melting temperature from elastic constants for these compounds.

Keywords: Y_3InC and La_3InC; first-principles method; mechanical properties; electronic properties; optical properties; thermodynamic properties

1. Introduction
Antiperovskite M_3BX crustals consist of special type of stable perovskite structure with a large number of ternary phases are really warmest materials. In crystallographic point of view, the M_3BX crystal structure are relate to the cubic structure of Cu_3Au. The formula M_3BX with M and B atoms are coincided at face center and 8 corners connecting with 12 near atoms respectively, while X coincide at the body center [1]. Due to the ability to tune it give rise in different electronic configuration with same structure by the variation of electron density is really attract much attention in modern era which opened a new horizon. Apart from this, there is much potentiality to explore it with promising physical properties to afford the modern demand. In recent years, scientists are found some interesting features with stable chemical composition of antiperovskite structure with the formula M_3BX. In view of that, it is been observed that several compounds with this antiperovskite structure such as Ti_3AlN [2], Ti_3AlC [3], Sc_3AlC [4], Sc_3AlN [5] and Sc_3InN [6] exhibits good mechanical properties. Furthermore, emphasized on to explore the possibility of ferromagnetisms or superconductivity several samples such as Ni_3GaC [7], Ni_3MgC, Ni_3CdC [8], Ni_3InC [9] Cr_3GaN and Cr_3RhN [10] are examined. Among the investigated Ni_3AC compounds with A =Al, Ga, In and Cd, only Ni_3CdC is a superconductor with T_c = 3.4 K [11].

Comparatively, some strong work manifest that antiperovskite metal-carbide shows some fascinating activities than nitrite because of carbon contain material as an impurity, expected to high ductility and strength [12]. In addition to that the hardness property of binary TiAl also increased when C was added and raised upto11 Gpa [13, 14].So, working on metal-carbide metal alloy is a way to get new advance material with greater benefits of physical and mechanical properties.

On the other hand, in the structure of M_3BX, all the potential elements of groups-ii and iv were substituted in A and B position and their characteristics also determined [1]. So, it's fascinating to search a new material to explore complicated task for understand the insight mechanism of A_3InC structure with the replacement of new element in A site. A paper on M_3InC (M=Y, La) has been published, where they show the preparation of material [15]. It is often complicated to find the dramatic changes in optical and electrical properties of such material, while rare earth elements is substituted in A-site on A_3BX structure. Again, the reactivity, fragility and other physical and mechanical properties are hidden experimental studies, under the extreme pressure of such sample. In that case, theoretical analysis is one of the key ways to clarify deep insight of such material for understanding macroscopic phenomena.

Therefore, the main focus of this work is to explore the physical properties of newly predicted M_3InC with M=Y and

La antiperovskite to investigate the role of Y and La inM_3InC structure, using first-principles calculations. Though many researchers have been studied on these types of antiperovskite crystal structures but no work has been found on M_3InC crystal structures yet.

2. Computational Methods

The first-principles investigations have been implemented using density functional theory (DFT) [16] based CASTEP code [17] within the GGA approximations through Perdew-Burke-Ernzerhof (PBE) exchange correlation energy function [18]. The electron-ion interactions have been explained by ultrasoft Vanderbilt-type pseudo-potentials [19]. The plane wave energy cut-off of 500 eV was applied for both phases to extend the wave functions. The structural parameters for both phases have been investigated through BFGS system [20] with a minimum energy. The Monkhorst-Pack grid [21] of 9×9×9 *k*-points have been used for Brillouin zone sampling. The convergence criteria were set with the 1×10^{-5}eV/atom of entire energy, 0.03 eV/Å of extreme force, 0.05 GPa of full stress and 0.001 Å of maximum displacement. The elastic stiffness constants of both phases have been performed using stress-strain method [22]. The Debye temperatures of both compounds have been calculated from elastic constant data.

3. Results and Discussion

3.1 Structural properties

The carbides antiperovskites M_3InC (where M=Y and La) possess the cubic crystal structure with $pm\bar{3}m$ (No. 221) space group and has 5 atoms per unit cell. The Wyckoff positions of atoms of these carbides antiperovskites are M: (0, 0.5, 0.5), In: (0, 0, 0) and C (0.5, 0.5, 0.5). The crystal structure of M_3InC (where M=Y and La) is shown in Fig.1.

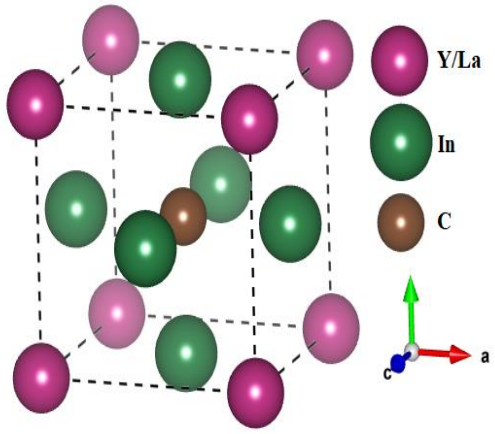

Fig 1: Crystal structure of M_3InC (where M=Y and La).

By minimizing the energy and force convergence, we have calculated the structural parameters. The calculated structural parameters such as lattice parameter a_0, cell volume V_0 and bulk modulus B_0 are presented in Table 1 with the available experimental data [15]. The optimized lattice parameters evident a good agreement with experimental data with some deviations. These deviations occurred by the temperature-dependence lattice parameters and GGA process [23]. Also the over estimation of the lattice parameters are the common factor of GGA based calculations.

Table 1: Calculated lattice parameter a_0 (Å), cell volume V_0 (Å^3) and bulk modulus B_0 of M_3InC (where M=Y and La).

Compound	a_0			V_0	B_0
	This work	Expt. [1]	Deviation (%)		
Y_3InC	4.995	4.902	1.897	124.625	100.861
La_3InC	5.299	5.193	2.04	148.793	58.107

3.2 Elastic properties

Elastic constants are essential parameters for a compound. These are used to investigate the stability, stiffness, ductility, brittleness and anisotropy properties of compound. There are only three independent elastic constants: C_{11},, C_{12} and C_{44} for cubic carbide antipervskites M_3InC (where M=Y and La). The elastic constants of M_3InC have been attained by using the stress-strain function according to Hook's law [24] at T=0 K and P=0 GPa. Second order elastic constants have been used to calculate the bulk modulus, Young's modulus, shears modulus, Pugh's ratio and Poisson's ratio of M_3InC. We have also calculated the Cauchy's pressure C_P and Zener's anisotropy index *A*. The calculated elastic constants C_{ij}, bulk modulus *B*, shear modulus *G*, Young's modulus *E*, Cauchy's pressure C_P, Pugh's ratio *B/G*, Poisson's ratio *v* and Zener's anisotropy index *A* of M_3InC are predicted in Table 2. The elastic constants C_{ij} of M_3InC are positive and satisfy the Born stability criteriaC_{11}-C_{12}>0, C_{44}>0 and C_{11}+2C_{12}>0 [25] indicating the mechanical stability of M_3InC under study. For our both compounds the value of *B* is larger than *G* which also indicates the mechanical stability of M_3InC [26]. Stress and strain ratio defined as Young's modulus also known as tensile modulus, *E*. The value of *E* calculated by 9*BG*/(3*B*+*G*) measures the stiffness behavior of the compound. The large value of *E* denotes the more stiffness characteristics of a compound [27]. Thus, Y_3InC is stiffer than La_3InC.

The Cauchy's pressure $C_P = C_{12}$-C_{44} concluded by Petti for [28] describes the brittleness/ductility of solids. The negative (positive) value of Cauchy's pressure indicates the brittle (ductile) characteristics of a compound. The brittle/ductile characteristics can also be understood by Pugh's ratio *B/G* [29] and Poisson's ratio *v*= (3*B*-*E*)/6*G* [30]. The high value of Pugh's ratio (*B/G*>1.75) and Poisson's ratio (*v*>0.26) shows ductility of a compound whereas for low values (*B/G*<1.75 and *v*<0.26) the compound will be brittle. According to Cauchy's pressure C_P, Pugh's ratio *B/G* and Poisson's ratio *v*, both compounds show the brittleness characteristics under study. It is also shown that Y_3InC has the more brittleness characteristics than La_3InC.

The important quantity which assesses the strength of a crystal known as Peierls stress of dislocations can be calculated using the shear modulus *G* and Poisson's ratio *v* by the following equation [31]:

$$\sigma_p = \frac{2G}{1-v} exp\left(-\frac{2\pi d}{b(1-v)}\right) \quad (1)$$

Where *b* is the Burgers vector and *d* is the interlayer distance between two glide planes. The calculated values of Burgers vector and interlayer distance with Peierls stress are listed in Table 2. Several MAX phases with Peierls stresses in the

range 0.74–0.98 GPa have the dislocation movement facilities whereas in some binary carbides with Peierls stresses in the range 17.46–22.87 GPa have no dislocation movement [32]. The calculated values of Peierls stresses for our both compounds possess the intermediate values between MAX phases and binary carbides which indicating the expectation of dislocation movement of Y_3InC and La_3InC.

The Zener's anisotropy factor $A=2C_{44}/(C_{11}-C_{12})$ [33] investigates the isotropic or anisotropic characteristics of a compound. The unit values of A shows the isotropic characteristics whereas deviation from unity measures the degree of elastic anisotropy of a compound. Thus, from Table 2, it is seen that both compounds are elastically anisotropic in nature. It is also seen that Y_3InC has high anisotropic characteristics whereas La_3InC possesses the lightly anisotropic characteristics.

Table 2: Calculated elastic constants C_{ij}, bulk modulus B, shear modulus G, Young's modulus E, Cauchy's pressure C_p, Pugh's ratio (B/G), Poisson's ratio ν and Zener's anisotropy factor A of M_3InC (where M=Y and La).

Compound	C_{11}	C_{12}	C_{44}	B	G	E	C_p	B/G	ν	b	d	σ_p	A
Y_3InC	183.05	32.59	56.84	82.75	63.59	151.8	-24.2	1.30	0.19	4.90	2.45	3.3	0.76
La_3InC	102.79	31.15	35.02	55.03	35.39	87.4	-3.87	1.55	0.23	5.19	2.59	1.6	0.98

3.3 Mulliken bond population and Vickers hardness

We have calculated the Mulliken bond population to studied the important mechanical properties such as Vickers hardness of M_3InC (where M=Y and La). The values of hardness measure the ability to resist plastic deformation of the materials. The relevant formula to calculate the hardness using Mulliken bond populations is given by [34, 35]:

$$H_v = \left[\Pi\left(H_\upsilon^\mu\right)^{\eta^\mu}\right]^{1/\Sigma\eta^\mu} \quad (2)$$

Where H_v^μ denotes for individual bond hardness and η^μ is the number of μ -type bond.

The individual bond hardness H_v^μ is calculated by the following equation:

$$H_v^\mu = 740\left(P^\mu - P^{\mu'}\right)(v)_b^{\mu\,-5/3} \quad (3)$$

Here P^μ is the Mulliken bond overlap population of the μ-type bond, $P^{\mu'} = \eta_{free}/V$ (where η_{free} =number of free electrons) is the metallic population, v_b^μ is the bond volume of μ -type bond. The calculated hardness values for our both compounds are tabulated in Table 3.

Table 3: Calculated bond, bond number n^μ, bond overlap population P^μ, bond length d^μ, bond volume v_b^μ (Å^3) and Vickers hardness H_v^μ (GPa) of μ -type bond, metallic population $P^{\mu'}$ and H_v (GPa) of M_3InC (where M=Y and La)

Compound	Bond	n^μ	d^μ	P^μ	$P^{\mu'}$	v_b^μ	H_v^μ	H_v
Y_3InC	C-Y	3	2.4975	0.89	0.0202	41.5417	1.29	1.29
La_3InC	C-La	3	2.6494	0.55	0.0363	49.59	0.57	0.57

From table, it is seen that C-Y bonds in Y_3InC have highest hardness with lower value of bond length than that of C-La bonds in La_3InC with larger value bond length. This table also shows that both compounds are relatively soft materials and La_3InC possesses the more softness properties than Y_3InC.

3.4 Electronic properties

The electronic properties play an important role to separate the materials to metal or to semiconductor or to insulator [36]. In the present investigation, we have calculated the band structure of Y_3InC and La_3InC as well as total and partial density of states. The calculated band structures have shown in Fig. 2. The band structures have studied in X-R-M-Γ-R high symmetry point in the first Brillouin zone. Further, the band structures have calculated within -9 to 6 eV energy range. The horizontal dotted line between valence band and conduction band at zero energy consider the Fermi level. The band structures show that some sub-bands are crossed the Fermi level at Γ Points for Y_3InC and at R and Γ points for La_3InC. Therefore, we conclude that the band structures have no band gap between two (valence and conduction) bands. For the above reason, we conclude that both materials reveal metallic nature. The calculated total and partial density of states have displaced in Fig. 3. The valence bands of total density of states show a first peak at around -14 eV and the long peaks mainly arise from In 4*d* states for Y_3InC. The second shot type peak shows at around -8.5 eV, which further comes from admixture of C 2*s* and Y 4*d* (or La 5*d*) states. A forbidden energy gaps of about -3 eV shows between the long and short peaks. The third peak shows around -5 eV and another forbidden energy gap shown between -8 to -5 eV energy ranges. The region between -4 eV to Fermi level mainly comes from the effect of C 2*p* and Y 4*d* states with admixture of In 4*d* states. The conduction band of total density of states shows two peaks that further arise for the contribution of Y 4*d* (or La 5*d*) with admixture of C 2*p* states.

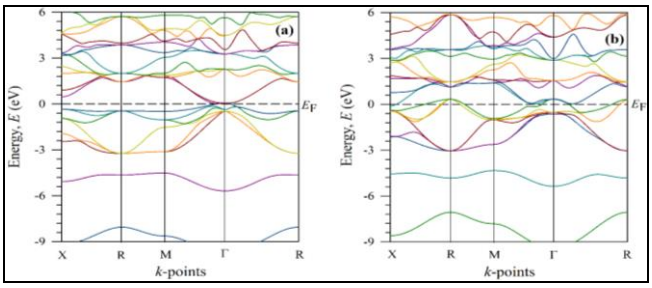

Fig 2: Electronic band structure of (a) Y_3InC and (b) La_3InC.

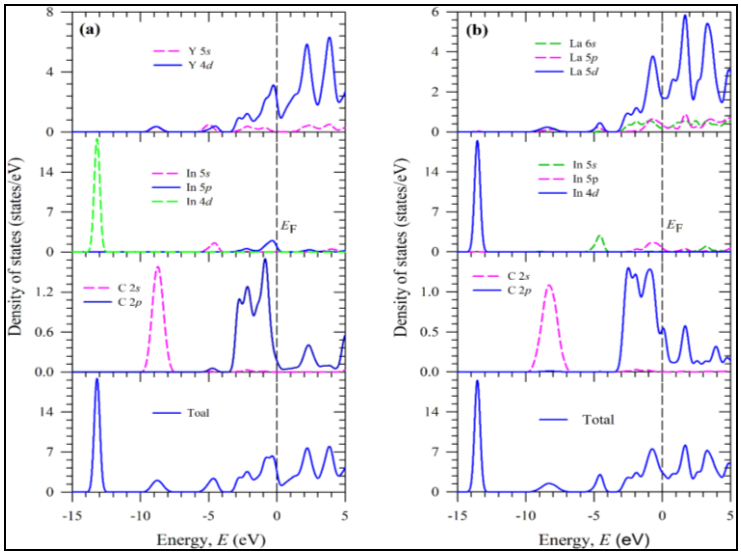

Fig 3: Calculated total and partial density of states (a) Y_3InC and (b) La_3InC.

The overall total and partial density of states in valence and conduction bands is similar for Y_3InC and La_3InC. The calculated total density of states are 3.4061 states/eV and 3.4047 states/eV, respectively.

3.5 Optical properties

The studies of optical properties of a material expose the different behavior of the compound in the field of incident electromagnetic radiation. The optical behavior of a material in visible region is very crucial for optoelectronic apparatus. In present study, we have investigated the dielectric function, reflectivity, refractive index, conductivity, absorption coefficient and loss function of Y_3InC and La_3InC. The dielectric function related with frequency dependent equation $\varepsilon(\omega) = \varepsilon_1(\omega) + i\varepsilon_2(\omega)$. The real part of this equation obtained by using the Kramers-Kronig transformation and related with Eqs. 49 to 54 in ref [37]. The second part (imaginary part) further related with the equation as follows [37].

$$\varepsilon_2(\omega) = \frac{2e^2\pi}{\Omega\varepsilon_0}\sum_{k,v,c}|\psi_k^c|u.r|\psi_k^v|^2\,\delta(E_k^c - E_k^v - E) \qquad (4)$$

Where, u and Ω are reveals the polarization of the incident electric field and the unit cell volume, ω and e are called the frequency of light and the charge of electron, ψ_k^c and ψ_k^v are reveals the conduction band wave function and the valence band wave function at K respectively.

Since the present studied materials denote metallic nature (confirmed from band structure and DOS results), we have used a Drude term (plasma frequency 3 eV and Drude damping 0.05 eV) for analysis of dielectric function [38]. The present investigation for optical function of Y_3InC and La_3InC have displaced in Fig. 4. The investigation represents here up to incident photon energy 45 eV for all optical functions. For all optical calculations a 0.5 eV value of Gaussian smearing have been used.

The calculated real and imaginary parts of dielectric function have shown in Fig. 4(a). The real part shows that it starts with negative value then goes towards the positive that indicates the Drude like behavior. The Drude behavior further indicates the metallic nature of Y_3InC and La_3InC. The imaginary part starts with positive value and decrease in IF and visible region and reaches zero at around 8 eV. This also indicates the metallic nature for present investigated compounds and this correspond to the energy in which absorption shows sharp drop and refractive index goes toward zero photon energy.

The complex and real part of refractive index have shown in Fig. 4(b). The real part of both compounds almost similar and have start at zero energy. The static values of refractive index are 6.84 and 7.83 for Y_3InC and La_3InC, respectively. The refractive index is high in IF and visible region and reaches zero energy at around 9 eV. The imaginary part also known as complex refractive index and measures the amount of absorption loss of an EM radiation. The values of complex refractive index for both materials further similar up to energy 0 to 12.6 eV and reveals the same concentrated materials. Moreover, both the materials strike same amount of EM radiations.

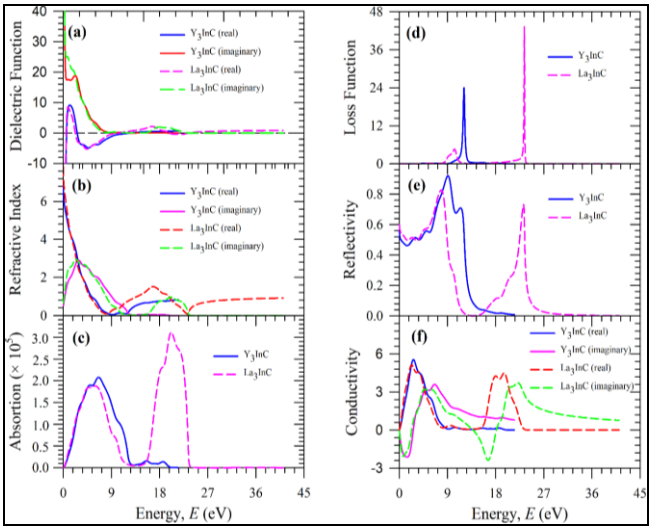

Fig 4: The frequency dependent (a) dielectric functions, (b) refractive index, (c) absorption coefficient, (d) loss function, (e) reflectivity and

(f) optical conductivity of Y_3InC and La_3InC along [100] polarization direction.

The calculated absorption spectra of Y_3InC and La_3InC have shown in Fig. 4 (c). From the Figure it is manifest that the absorption starts at zero energy that indicates the metallic nature. The absorption between 0 and 12.6 eV is similar and after 12.6 the contribution of Y_3InC is negligible whereas Y_3InC shows maximum absorption at 19.8 eV.

The calculated loss functions have shown in Fig. 4 (d). The loss function show peaks at 12.6 eV and 23.4 eV for Y_3InC and La_3InC. The energy 12.6 eV corresponds to the energy in which reflectivity shows maximum for Y_3InC and La_3InC, and La_3InC further shows second peak at 23.4 eV. The peaks energy 12.6 eV and 23.4 eV indicate the bulk plasma frequency and these points' further reveals the maximum energy loss points.

The higher reflectivity appears at around 7.2 eV and 9 eV for Y_3InC and La_3InC (shown in Fig. 4(e)). These correspond to the energy in which the conductivity falls to zero and absorption quality is good. The La_3InC compound show good reflectivity in higher energy also. The overall reflectivity within 0 to 14.4 eV is similar for both compounds. For the reason we conclude that Y_3InC and La_3InC are promising material to be use as a reflector material in the UV energy region.

The good conductivity shows in visible region and around 9 eV the less conductivity has also shown (Fig. 4(f)). The higher reflectivity around 18 eV further has shown good for La_3InC. The overall conductivity value indicates that the materials La_3InC is more suitable to use in electrical conductor than Y_3InC for visible and UV regions.

3.6 Thermodynamic Properties

The Debye temperature $\theta(D)$ is a momentous part in thermodynamic which denotes the minimum temperature at which the highest frequency mode of vibration is occurred. It also gives the many others physical properties including specific heat, melting point, thermal expansion etc. of a material. The Debye temperature $\theta(D)$ of a material is calculated by using the following equation [39]:

$$\theta(D) = \frac{h}{k_B}\left(\frac{3N}{4\pi V}\right)^{\frac{1}{3}} \times v_m \quad (5)$$

Where h is the plank constant, k_B is the Boltzman constant, N is the number of atoms per unit cell, V is the volume of unit cell and v_m is the average sound velocity.

The average sound velocity v_m is obtained by the following equation [40]:

$$v_m = \left[\frac{1}{3}\left(\frac{2}{v_t^3} + \frac{1}{v_l^3}\right)\right]^{-\frac{1}{3}} \quad (6)$$

Where v_t and v_l are representing transverse and longitudinal sound velocity respectively which are calculated by the Navier's equation [41]:

$$v_t = \left(\frac{G}{\rho}\right)^{\frac{1}{2}} \quad (7)$$

$$v_l = \left(\frac{3B+4G}{3\rho}\right)^{\frac{1}{2}} \quad (8)$$

Where ρ is the mass density per unit volume of the unit cell and B and G are the bulk and shear modulus respectively. For our both phases the calculated density ρ, transverse v_t, longitudinal v_l and average v_m sound velocities and Debye temperature $\theta(D)$ are tabulated in Table 4.The calculated values show that Y_3InC has the higher value of Debye temperature than that of La_3InC. Thus, Y_3InC has the higher ability to store energy from La_3InC.

The capability to conduct heat is called thermal conductivity of a solid material. Thermal conductivity which is increased with decreasing the temperature up to a certain limit defined as the minimum thermal conductivity of that solid material. The value of minimum thermal conductivity is obtained by Clarke expression using following formula [42]:

$$K_{min} = K_B v_m \left(\frac{M}{N\rho N_A}\right)^{-\frac{2}{3}} \quad (9)$$

Here N_A is the Avogadro number. The calculated values of minimum thermal conductivity for our both phases are listed in Table 4. The calculated values show that Y_3InC has the higher value of minimum thermal conductivity than that of La_3InC. Thus, the values of Debye temperature and minimum thermal conductivity indicating our calculations follow thumb rule [43]. It is also seen that La_3InC has more advantages to use as a thermal barrier coating (TBC) material due to the low values Debye temperature and minimum thermal conductivity than that of Y_3InC [44].

The temperature at which solid phase turns into liquid phase at atmospheric pressure is called melting temperature, T_m of a material. For cubic crystal structures melting temperature is obtained by the following equation [45].

$$T_m = 553 + 5.91C_{11} \quad (10)$$

For these both phases the melting temperatures are tabulated in Table 4 which indicates that La_3InC has more convenient effect to melt down than Y_3InC.

Table 4: Calculated density ρ (in gm/cm^3), transverse v_t, longitudinal v_l and average v_m sound velocities (in m/s), Debye temperature $\theta(D)$ (in K), Minimum Thermal Conductivity K_{min} (in Wm^{-1}K^{-1}) and melting temperature T_m (in K) of Y_3InC and La_3InC.

Compound	ρ	v_t	v_l	v_m	θ_D	K_{min}	T_m
Y_3InC	5.93	3274.67	5315.29	3612.91	368.62	0.56	1634.83
La_3InC	5.53	2529.75	4299.31	2803.71	269.65	0.40	1160.49

4. Conclusions

In summary, the brief discussion of physical properties including structural, mechanical, electronic, optical and thermodynamic properties of In-based carbide antipervskites

M_3InC (where M=Y and La) have been performed using the density functional theory with plane-wave pseudo potentials. The physical properties for these phases are investigated at first time. The optimized lattice parameters show a slight variation 1.897% and 2.04% from experimental values indicating the good satisfaction of our calculations. The calculated elastic constants gratify the required born stability conditions which indicates the mechanical stability of Y_3InC and La_3InC. The study of Cauchy pressure, Pugh's ratio and Poisson's ratio reveal the brittleness characteristics of Y_3InC and La_3InC. The low values of Peierls stresses indicate the expectation of dislocation movement of Y_3InC and La_3InC. The deviation of Zener's anisotropy index *A* from unity show the anisotropic properties for these phases. The calculated values of Mulliken bond overlap population and Vickers hardness indicate that both phases are very soft materials with compare to Diamond. The absence of band gap at Fermi level in band structures and high values of DOS at Fermi level show the metallic behavior of Y_3InC and La_3InC. The calculated total density of states are 3.4061 states/eV and 3.4047 states/eV, respectively show the similar metallic characteristics. The large negative values of dielectric function (real part) show the Drude like behavior also indicating the metallic nature of Y_3InC and La_3InC.The reflectivity spectra shows that Y_3InC and La_3InC are promising as a reflector material in the UV energy region. The conductivity spectra indicate both phases are good conductors whereas La_3InC is more suitable than Y_3InC to use for visible and UV regions. The calculations of thermodynamic properties have been performed depending on elastic constants. The values of Debye temperature and minimum thermal conductivity show that both phases can be use as thermal barrier coating (TBC) material whereas La_3InC has more advantages that of Y_3InC. The melting temperature shows that both phases have high melting temperature and La_3InC has more convenient effect to melt down than Y_3InC.

References

1. Mikhaylushkin AS, Höglund C, Birch J, Czigány Z, Hultman L, Simak SI. *et al*. Stability of the ternary perovskites Sc_3EN (E=B, Al, Ga, In) from first principles, Physical Review B230, 2009, p. 134107.
2. Schuster JC, Bauer J. The ternary system titanium-aluminum-nitrogen, Journal of Solid State Chemistry, 1984, 53:260.
3. Tian WH, Nemoto M. Crystallography and morphology of $D0_{23}$-$Al_{11}Ti_5$ precipitation in Ag-modified $L1_2$-Al_3Ti, Intermetallics8, 2000, p. 835.
4. Nowotny VH, Strukturchemie einiger Verbindungen der Übergangsmetalle mit den elementen C, Si, Ge, Sn, Solid State Chemistry, 1971, 5:p. 27.
5. Höglund C, Birch J, Beckers M, Alling B, Czigány Z, Mücklich A. *et al*. Sc_3AlN – A New Perovskite, European Journal of Inorganic Chemistry, 2008, p. 1193.
6. Kirchner M, Schnelle W, Wagner FR, Niewa R. Preparation, crystal structure and physical properties of ternary compounds (R_3N) In, R=rare-earth metal, Solid State Sciences, 2003, 5:1247.
7. Bannikov VV, Shein IR, Ivanovskii AL. Structural, elastic and electronic properties of new antiperovskite-like ternary nitrides $AlNNi_3$, $GaNNi_3$ and $InNNi_3$ as predicted from first principles, Computational Materials Science, 2010, 49:457.
8. Wu SQ, Hou ZF, Zhu ZZ. Elastic properties and electronic structures of $CdCNi_3$: A comparative study with $MgCNi_3$, Solid State Sciences, 2009, 11:251.
9. Wu SQ, Hou ZF, Zhu ZZ. Electronic structure and magnetic state of $InCNi_3$, Physica B: Condensed Matter, 2008, 403:4232.
10. Wiendlocha B, Tobola J, Kaprzyk S, Fruchart D. Electronic structure, superconductivity and magnetism study of Cr_3GaN and Cr_3RhN., Journal of Alloys and Compounds, 2007, 442:289.
11. Uehara M, Amano T, Takano S, Kôri T, Yamazaki T, Kimishima Y. Chemical pressure effect on the superconductor $MgCNi_3$. Physica C: Superconductivity, 2006, 440:6.
12. Yuki I, Amano N, Uozumi M, Inui H, Yamaguchi M. Effect of Nitrogen Addition on the Microstructure and Mechanical Properties of Cast gamma Titanium Aluminide Alloys, J Jpn. Inst. Met, 1994, 58:564.
13. Van Thyne RJ, Kessler HD. Influence of Oxygen, Nitrogen, and Carbon on the phase relationships of the Ti-Al system, JOM, 1954, 6:93.
14. Wilhelmsson O, Palmquist JP, Lewin E, Emmerlich J, Eklund P, Persson POÅ. *et al*. Deposition and characterization of ternary thin films within the Ti–Al–C system by DC magnetron sputtering, Journal of Crystal Growth, 2006, 291:290.
15. Jing-Tai Zhao, Zhen-Chao Dong JT, Vaughey Jerome, Ostenson E, John D Corbett. *et al*. Synthesis, structures and properties of cubic R_3In and R_3InZ phases (R =Y, La; Z = B, C, N, 0): The effect of interstitial Z on the superconductivity of La_3In, Journal of Alloys and Compounds, 1995, 230:1.
16. Kohn W, Sham LJ. Self-Consistent Equations Including Exchange and Correlation Effects, Phys. Rev. A, 1965, 140:1133.
17. Clark SJ, Segall MD, C.J. Pickard, P.J. Hasnip, M.I. Probert, K. Refson and M.C. Payne, First principles methods using CASTEP, Z. Kristallog, 2005, 220:567.
18. Perdew JP, Burke K, Ernzerhof M. Generalized gradient approximation made simple, Phys. Rev. Lett, 1996, 77:3865.
19. Vanderbilt D. Soft self-consistent pseudopotentials in a generalized eigenvalue formalism, Phys. Rev. B, 1990, 41:7892.
20. Pfrommer BG, Cote M, Louie SG, Cohen ML. Relaxation of crystals with the quasi-Newton method, J Comput. Phys, 1997, 131:233-240.
21. Monkhorst HJJD. Pack, Special points for Brillouin-zone integrations, Phys. Rev. B, 1976, 13:5188.
22. Kang J, Lee EC, Chang KJ. First-principles study of the structural phase transformation of hafnia under pressure, Phys. Rev. B, 2003, 68:054106.
23. Zhu YD, Yan MF, Zhang XY, Zhang CS. First-principles investigation of structural, mechanical and electronic properties for Cu-Tiintermetallics, Computational Materials Science, 2016, 123:70.
24. Nye JF. Proprietes Physiques des Materiaux, Dunod,

Paris, 1961.
25. Born M. On the stability of crystal lattices. I, Math. Proc. Cambridge Philos. Soc, 1940, 36:160.
26. Salma MU, Atikur Rahman Md. Study of structural, elastic, electronic, mechanical, optical and thermodynamic properties of $NdPb_3$ intermetallic compound: DFT based calculations, Computational Condensed Matter, 2018, 15:42.
27. Okoye CMI. Structural, elastic and electronic properties of new antiperovskite-typesuperconductor ZnNNi3 from first-principles, Physica B, 2010, 405:1562-1570.
28. Pettifor DG. Theoretical predictions of structure and related properties of intermetallics, Materials Science and Technology, 1992, 8:345.
29. Pugh SF. Relations between the elastic moduli and the plastic properties of polycrystalline pure metals, Philosophical Magazine, 1954, 45:823-843.
30. Frantsevich N, Voronov FF, Bokuta SA. Elastic Constants and Elastic Moduli of Metals and Insulators Handbook, edited by I. N. Frantsevich, Naukova Dumka, Kiev, 1983, p. 60.
31. Lu G. The Peierls-Nabarro Model of Dislocations: a Venerable Theory and its Current Development, Handbook of Materials Modeling, edited by S. Yip (Springer, Amsterdam, 2005, p. 1.
32. Music D, Schneider JM. Elastic properties of $Sr_{n+1}TinO_{3n+1}$phases (n = 1–3, ∞) J. Phys.: Condens. Matter, 2008, 20:055224.
33. Zener C. Elasticity and Anelasticity of Metals, University of Chicago Press, Chicago, 1948.
34. Gao F. Theoretical model of intrinsic hardness, Phys. Rev. B, 2006, 73:132104.
35. Gou H, Hou L, Zhang J, Gao F. Pressure-induced incompressibility of ReC and effect of metallic bonding on its hardness, Appl. Phys. Lett, 2008, 92, p. 241901.
36. Wen-Cheng Hu, Yong Liu, De-Jiang Li, Xiao-Qin Zeng, Chun-Shui Xu. First-principles study of structural and electronic properties of C14-type Laves phase Al_2Zr and Al_2Hf, Comput. Mater. Sci, 2014, 83:27.
37. Materials Studio CASTEP Manual Accelrys, 2010. Available at http://www.tcm.phy.cam. ac.uk/castep/documentation/WebHelp/CASTEP.html
38. Saniz R, Lin Hui Ye, Shishidou T, Freeman AJ. Structural, electronic, and optical properties of $NiAl_3$: First principles calculations, Phys. Rev. B, 2006, 74:014209.
39. Aydin Sezgin, Mehmet Simsek. First-principles calculations of MnB_2, TcB_2, and ReB_2 within the ReB_2-type structure, Physical Review B. 2009; 80(13):134107.
40. Schreiber E, Anderson OL, Soga N. Elastic Constants and their Measurements, McGraw-Hill, New York, 1973.
41. Anderson OL. A simplified method for calculating the debye temperature from elastic constants, Journal of Physics and Chemistry of Solids, 1963; 24:909.
42. Clarke DR. Materials selection guidelines for low thermal conductivity thermal barrier coatings, Surface and Coatings Technology, 2003, 163:67.
43. Salma MU, Md Atikur Rahman. Physical Properties of $ThCr_2Si_2$-type Rh-based compounds ARh_2Ge_2 (A=Ca, Sr, Y and Ba): DFT Based First-principles investigation, International Journal of Modern Physics B, 2018.
44. Chowdhury UK, Rahman MA, Rahman A, Das PK, Salma MU, Ali MS. *et al*. Physica C: Superconductivity and its applications, 2018.
45. Mehl MJ, Klein BM, Papaconstantopoulos DA. First principles calculations of elastic properties of metals, 1994, 1.